CFD MODEL FOR JET FAN VENTILATION SYSTEMS

Kailash C. Karki, Suhas V. Patankar
Innovative Research, Inc.
3025 Harbor Lane N., Suite 300
Plymouth, MN 55447 USA

Elana M. Rosenbluth, Sam S. Levy
Parsons Brinckerhoff
One Penn Plaza
New York, NY 10119 USA

published in
Proceedings of the 10th International Symposium
on Aerodynamics and Ventilation of Vehicle Tunnels
Principles, Analysis and Design
1–3 November 2000, Boston, USA
Organized and sponsored by BHR Group Limited.

Synopsis
The development and validation of a computational fluid dynamics model for a longitudinal ventilation system using jet fans has been presented. The model includes component models for turbulence, fire, radiation, smoke, and jet fan. It has been validated using the data from the Memorial Tunnel Fire Ventilation Test Program. The predictions are in good quantitative agreement with the test data in the far-field region (60 m away from the fire) of the tunnel.

1 INTRODUCTION

Background. Mathematical models based on computational fluid dynamics (CFD) are becoming popular as predictive tools in fire safety area for describing fire spread and smoke movement. They are used, for example, to assess the effectiveness of alternative ventilation strategies and to get answers to a range of "what if?" questions. To further increase the use of these models in the design methods for fire safety systems, a number of key issues need to be addressed. These include:

- Definition of the scope of a model and its audience. This process will help in establishing suitable criteria for the selection and evaluation of the component models (e.g., models for turbulence, combustion, radiation, and smoke) and for the evaluation of the overall fire model.
- Validation of the component models and the overall fire model. The validation studies must demonstrate that the accuracy of predictions is sufficient to meet the stated objective of the model. There is need for well-defined data, from laboratory experiments and full-scale tests, for model validation.
- Ease of use. CFD fire models are often based on general-purpose computer programs and require extensive training. These models will gain wider acceptance in the fire safety area if they are customized, in terms of pre- and post-processing and component models, to the problems involving fire.

These issues in the context of models for tunnels were addressed in the Memorial Tunnel Fire Ventilation Test Program (MTFVTP) (Ref. 1). The overall objective in this program was to evaluate the smoke and temperature management capabilities of various ventilation systems for road tunnels and to provide reliable data for validating analytical/computational models for fire emergencies. The Memorial Tunnel, an abandoned road tunnel in West Virginia, was modified, retrofitted with new ventilation equipment, and instrumented to evaluate ventilation system performance during full-scale testing as a function of system type and capacity, and fire size. Ventilation systems tested included longitudinal ventilation using jet fans, natural ventilation, full transverse ventilation, partial transverse ventilation, and partial transverse ventilation supplemented with special extraction techniques. A total of 98 full-scale tests were carried out with fires ranging in intensity from 10 to 100 MW.

The test program comprised four phases. The first three phases addressed test program development, test facility design and construction, testing, and data evaluation. Phase IV focused on the development and validation of a customized computational model based on CFD for tunnel ventilation. Data from the full-scale fire tests was used for validation of the model.

The computational model developed in Phase IV of the Memorial Tunnel Test program (henceforth referred to as the tunnel ventilation model) is applicable to different ventilation modes, including longitudinal ventilation using jet fans, transverse ventilation, and natural ventilation. This model is geared towards individuals (analysts, designers, and tunnel operators) concerned with fire/life safety in tunnels. The primary objective established for the model is the ability to simulate the interactive effects of a tunnel fire and the ventilation system to determine the unsafe regions of the tunnel, that is, the regions where the hazardous effects of the fire (smoke and high temperature) are confined, and how these regions are affected by the ventilation system configuration, capacity, and operation.

The tunnel ventilation model is based on the general-purpose CFD code COMPACT-3D (Ref. 2). It employs the buoyancy-augmented k-ε model to represent the turbulent transport and includes component models for jet fans, ventilation ducts, fire, radiation heat transfer, and smoke. The present paper deals with the validation and application of this model for longitudinal ventilation systems with jet fans. The details for transverse ventilation systems are available in Levy et al. (Ref. 3) and in the MTFVTP Phase IV report (Ref. 4).

Prior Studies. A limited number of field models for longitudinal ventilation systems using jet fans are available in the literature. Armstrong et al. (Ref. 5) have presented comparison of results from a CFD model with experiments for a $1/15^{th}$ size model of a tunnel 8.25 m. in diameter. The geometry of the tunnel is axisymmetric and the flow is isothermal. The predicted results are in good agreement with the experimental data and results from an analytical model. Tabarra and co-workers (Refs. 6, 7) have studied jet fan-induced flows in rectangular tunnels. They include the effect of the proximity of a fan from tunnel wall on airflow characteristics. These studies are also limited to isothermal flows. Again, the results from the CFD model are in good agreement with the experimental data. Recently Miles and Kumar (Ref. 8) have reported limited results from the CFD fire model TUNFIR for selected longitudinal tests from the Memorial Tunnel test program. The predicted results are in reasonable agreement with the test data.

Present Contribution. This paper describes the tunnel ventilation model and its validation for longitudinal ventilation systems using jet fans. The validation is based on the data from the Memorial Tunnel test program as well as data from other sources. The model was also used to

calculate isothermal flows in prototype tunnels to demonstrate that it correctly reproduces the established jet fan characteristics. To simulate the Memorial Tunnel tests, special care was taken to ensure that all important aspects of the actual tests were properly incorporated in the model. These included, for example, the details of the instrument trees, the wall roughness, the prevailing wind conditions during the tests, and the thermal conditions for the tunnel walls. Since there are uncertainties associated with a number of input parameters (e.g., the heat release rate), parametric runs were also made to evaluate the sensitivity of the predicted results to changes in these input parameters.

The paper is organized as follows. The next section gives the details of the computational model. Section 3 provides a brief description of the Memorial Tunnel test program. Section 4 discusses the approach for model validation, the tests cases, and the results of various simulations.

2 DESCRIPTION OF THE TUNNEL VENTILATION MODEL

The tunnel ventilation model is based on the buoyancy-augmented k-ε turbulence model and includes component models for representing jet fans, fire, radiation heat transfer from the fire, and smoke movement. These component models were implemented in the general-purpose CFD software package COMPACT-3D. The details of the mathematical model and the numerical method are presented in this section.

2.1 Considerations in Model Development

Longitudinal ventilation systems employing jet fans are commonly associated with road tunnels serving uni-directional traffic. In the event of a fire, it is usually assumed that the traffic ahead of the fire will proceed to the exit portal and the traffic behind the fire will come to a stop. The ventilation system would be operated to force the smoke and hot gases in the direction of empty tunnel to provide a clear and safe environment behind the fire to evacuating people and fire fighters.

If the ventilation capacity is sufficient, all of the heated air and smoke will flow in the downstream direction. If ventilation is weak, the upper layers of heated air and smoke may flow in the opposite direction causing "backlayering." The occurrence of backlayering depends on many factors including the intensity of fire, the grade and geometry of the tunnel, and the velocity of the ventilating air approaching the fire. The ability of the longitudinal ventilation system to prevent backlayering is the current industry standard to measure the adequacy of the system for smoke control.

With these considerations in mind, the following objectives were established for the model:

- It is geared toward individuals—analysts, designers, and operators—concerned with fire/life safety in tunnels.
- It should be able to simulate the interactive effects of the tunnel fire and the ventilation system to determine the unsafe regions in the tunnel, that is, the regions where the hazardous effects of fire (smoke and high temperatures) are confined. In addition, it should be able to predict how these regions are affected by the ventilation system configuration, capacity, and operation. The ability to accurately predict the local details of flow and temperature fields was considered secondary.
- It should be able to predict the occurrence of backlayering.

2.2 General Form of the Governing Equations

The governing equations for the transport of mass, momentum, energy, turbulence parameters and other quantities can be cast, using the Cartesian tensor notation, in the following general form (Ref. 9):

$$\frac{\partial}{\partial t}(\rho\phi)+\frac{\partial}{\partial x_i}(\rho u_i\phi)=\frac{\partial}{\partial x_i}\left(\Gamma\frac{\partial\phi}{\partial x_i}\right)+S \tag{1}$$

where ϕ is the general dependent variable, ρ is the fluid density, Γ is the generalized diffusion coefficient, and S is the source term. The density is calculated from the perfect gas law. The expressions for the diffusion coefficients and the source terms appearing in the transport equations are well known [e.g., Cox (Ref. 10)] and are not presented here. The component models for fire, radiation, smoke, and jet fans introduce additional source terms in these equations; these details are presented in the appropriate sections on the component models.

2.3 Turbulence Model

Turbulence is modeled using the buoyancy-augmented k-ε model. In the k-ε model (Ref. 11), turbulence is represented by the turbulence kinetic energy k and its rate of dissipation ε. Both these parameters are governed by differential equations of the form as Eq. (1). The source terms for k and ε are given by:

$$S_k = P + G_B - \rho\varepsilon \tag{2}$$

$$S_\varepsilon = c_1(P + G_B)\frac{\varepsilon}{k} - c_2\rho\frac{\varepsilon^2}{k} \tag{3}$$

In the above equations, P is the turbulence production due to shear and G_B is the production due to buoyancy, given by

$$G_B = -\frac{\mu_t}{\sigma_T}\frac{1}{\rho}g_i\frac{\partial\rho}{\partial x_i} \tag{4}$$

where μ_t is the turbulent viscosity, σ_T is the turbulent Prandtl number for temperature, and g_i denotes the component of the gravitation acceleration along the coordinate direction i. The term G_B describes the exchange of turbulence kinetic energy with the potential energy of the system; it takes on opposite signs in the regions of stable and unstable stratification. This term is negative, acting to suppress turbulence, in regions where the stratified flow is stable. In regions of unstable stratification, this term is positive and leads to augmentation of turbulence.

The turbulent viscosity is given in terms of k and ε as

$$\mu_t = c_\mu\rho\frac{k^2}{\varepsilon} \tag{5}$$

and the turbulent diffusion coefficient for a scalar (e.g., temperature, species concentration) is calculated as

$$\Gamma = \frac{\mu_t}{\sigma_t} \tag{6}$$

where σ_t is the turbulent Prandtl or Schmidt number.

Treatment of a Wall Boundary. The wall function approach (Ref. 11) is used to eliminate the need to resolve the laminar sublayer. The standard expressions for momentum and convective heat/scalar fluxes are modified according to the recommendations of Jayatilleke (Ref. 12) to include the effect of wall roughness.

The turbulence kinetic energy at a near-wall grid point is calculated by solving its transport equation with diffusion flux to the wall set equal to zero. The near-wall value of the rate of dissipation is deduced by assuming that the length scale in this region varies linearly with the distance from the wall.

2.4 Representation of Fire

The fire is represented as a source of heat and mass. The model does not simulate the combustion process. Instead, the heat release rate due to combustion is prescribed as a volumetric heat source in a *postulated* fire region. Thus the model needs information on the flame size and shape and the volumetric heat release rate and its distribution. The heat release rate is computed from the rate of fuel consumption $\dot{m}_{fu}$, the heating value of the fuel H_{fu} and combustion efficiency η, as

$$Q = \dot{m}_{fu} H_{fu} \eta \tag{7}$$

In the fire region, additional source terms are included in the mass continuity and energy equations. For the continuity equation, the source term is calculated from the rate of fuel consumption. For the energy equation, the source term depends on the treatment of radiation heat transfer and is discussed in the next section.

2.5 Representation of Radiation Heat Transfer

The model includes two options for representing radiation transport. In the *radiative fraction* approach, thermal radiation in the participating medium is ignored and a fixed fraction of the total heat released in the fire is assumed to be lost to the surroundings without affecting the temperature distribution within the tunnel; the remaining energy is transported away by the fluid. Experiments on diffusion flames indicate that the radiation fraction typically lies in the range 0.2 to 0.4 (Ref. 13). With this treatment, the energy convected by the fluid is given by

$$Q_C = \dot{m}_{fu} H_{fu} \eta (1 - \chi_R) \tag{8}$$

where χ_R is the radiative fraction.

In the *detailed radiation treatment*, the six-flux model (Ref. 14) is used for calculation of thermal radiation in the participating medium. The entire heat released in the fire region is introduced as source in the energy equation, and the radiation model determines the amount of energy lost to the walls. This model needs additional information about the radiation properties

of the medium and the tunnel walls. Use of this model increases the computational effort and complexity, since additional equations must be solved to calculate the radiation fluxes.

A selected number of test cases were simulated using both these treatments for radiation heat transfer. The results, described in Ref. 4, indicated that the simplified radiative fraction approach met the objectives of the model. Therefore, all the results presented in this paper are based on the radiative fraction approach.

2.6 Representation of Smoke

The model solves a separate conservation equation for smoke. This equation contains a source term in the fire region to represent the rate of production of smoke. This source term is calculated from the specified rate of fuel consumption and the stoichiometric ratio for the fuel assuming complete combustion. Thus,

$$\dot{m}_{smoke} = \dot{m}_{fu}(1+s) f_{smoke} \tag{9}$$

where s is the stoichiometric ratio (kg of air/kg of fuel) for the fuel. In Eq. (9), a factor f_{smoke} has been introduced. The value of this factor depends on the interpretation of smoke: whether it is considered as the products of combustion or as the "particulate" smoke. For the former definition, f_{smoke} is unity; for the latter it can be interpreted as the smoke potential of the fuel.

It should be noted that due to the differences in the boundary conditions at the tunnel walls and the nature of the source terms, the distributions of temperature and the products of combustion, in general, would not be identical.

This model for smoke movement does not account for soot formation. A comprehensive soot model would require component models for soot formation and gas-phase chemistry; such a model was considered beyond the scope of the tunnel ventilation model.

2.7 Representation of Jet Fan

A jet fan is represented as a constant volumetric flow rate device. Here it should be recognized that the constant flow rate is applied only to the flow actually going through the jet fan. The flow *induced* by the jet fan in the entire tunnel is not held constant. Indeed, the interaction of the jet (produced by the jet fan) with the surrounding air determines how much flow gets induced in the tunnel. The induced flow also depends on the size, shape and length of the tunnel, wall roughness, and on the presence of flow obstacles.

A jet fan is simulated by a combination of sources and sinks. The specific details are as follows:

- The control volumes within the fan region are blocked-off, i.e., they are treated as solid. The diffusion coefficients for temperature and species concentrations in the fan region are set equal to zero so that there is no interaction between the fluid within the fan and the fluid on the outside.
- Mass and momentum sources (and sources for turbulence parameters, energy, and smoke) are introduced in the fluid control volumes adjacent to the discharge end of the fan. The strengths of the mass and momentum sources are determined from the fluid density at the intake end of the jet fan, the fan capacity, and the discharge velocity. The sources for k and ε are calculated using specified input for turbulent intensity and length scale at the jet fan intake. For the energy equation, the total enthalpy entering the fan from the intake end

is introduced as source at the discharge end. Thus, there is no energy addition within the jet fan. A similar practice is used for smoke.

- Mass sinks are introduced in the fluid control volumes next to the intake end of the fan.

2.8 Boundary Conditions

2.8.1 Tunnel Portals

The portals can be specified as inflow/outflow boundaries or as "free" boundaries with known values of pressure, depending on the physical situation being modeled.

At an inflow boundary, values of all variables are specified. At an outflow boundary, the diffusion flux is assumed to be zero and the normal velocity components are adjusted to ensure the overall conservation of mass. When the value of pressure is specified at a portal, the conditions within the tunnel determine whether the fluid enters or exits through portions of a portal. At the inflow points on a free boundary, the ambient values of temperature and other scalars are specified; at the outflow points, the diffusion flux is set equal to zero.

The model also has provision for the introduction of entrance loss and differential pressures at the portals to represent wind effects.

2.8.2 Tunnel Walls

At a solid-fluid interface, the wall-function approach is used. For the momentum equations, the no-slip condition is imposed on the solid surfaces. For species concentrations, the diffusion flux into the wall is zero. For temperature calculation, the value of temperature or heat flux can be specified on the walls.

The tunnel walls and internal blockages can be specified as hydraulically smooth or rough surfaces. As indicated earlier, the wall functions are suitably modified to account for the effect of wall roughness on momentum and heat transfer.

2.9 Numerical Solution Method

Here a brief overview of the numerical method used for the solution of the governing equations is presented; complete details are available in Refs. 2, 9, and 15.

The numerical method is based on the finite-volume formulation. A staggered grid arrangement is used for the location of the dependent variables. The scalar quantities (e.g., pressure, temperature, and species concentrations) are stored at the grid points, which are located at the centers of the control volumes, and the velocity components are located at the control-volume faces. This arrangement maintains strong coupling between the velocity and pressure fields and prevents the appearance of a checkerboard pressure field.

The model uses a Cartesian grid to represent the geometry; features that do not fit neatly in the grid are approximated using staircase steps. The Power-law scheme is used to represent the convection-diffusion terms in the conservation equations. The fully implicit scheme is used to discretize the unsteady term. The SIMPLER algorithm is used to calculate the pressure field.

The algebraic equations are solved using the line-by-line TriDiagonal-Matrix Algorithm (TDMA), supplemented by a block-correction procedure (Refs. 15, 16). In the line-by-line method, the TDMA is used to solve for ϕ's along a grid line (e.g., in the y-direction), by assuming that the ϕ's along the neighboring lines (i.e., in the x- and z-directions) are known from their latest values. This procedure is repeated for all the lines in one direction, and the procedure is repeated for the lines in the other two directions.

3 MEMORIAL TUNNEL FIRE VENTILATION TEST PROGRAM

3.1 Tunnel Configuration

The Memorial Tunnel is about 853 m long and has a constant 3.2 percent grade from south to north. The original tunnel had a full transverse type ventilation system with exhaust and supply fan chambers located above the north and south portals. An overhead air duct, formed by a concrete ceiling located above the roadway, was divided into supply and exhaust sections by a vertical concrete dividing wall. To facilitate longitudinal ventilation testing, the tunnel ceiling was removed and jet fans were installed in the crown of the tunnel. All the jet fans were identical. Each fan had a discharge area of 1.287 m^2 and a nominal volume flow rate of 42.94 m^3/s. The tunnel profile, cross sections, and jet fan arrangement are shown in Figure 1.

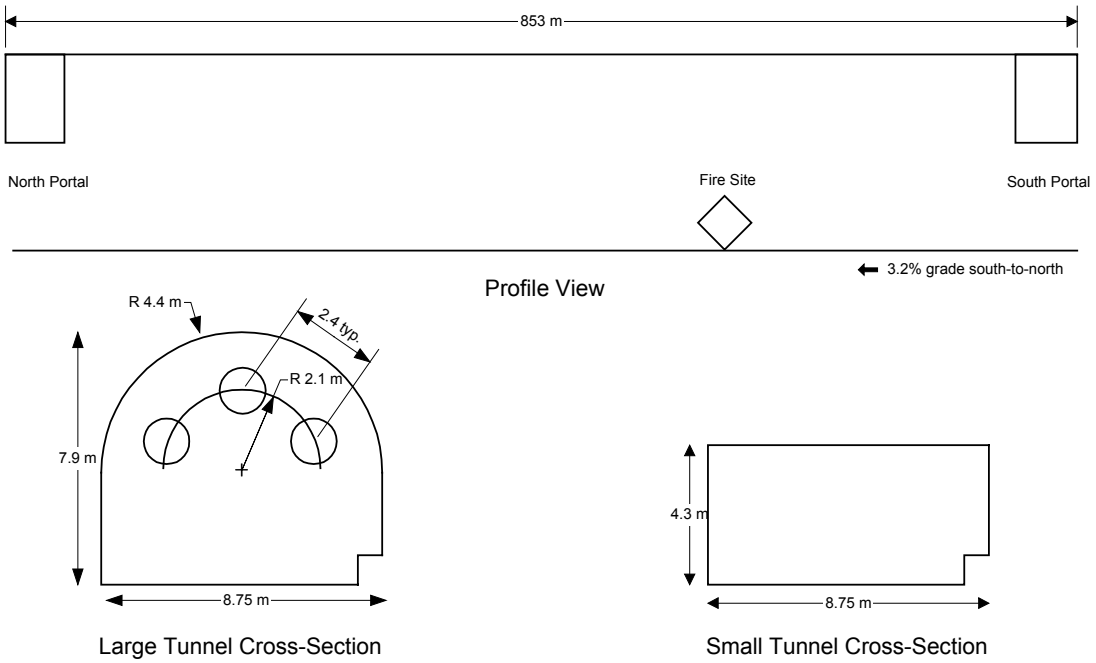

Figure 1 Memorial Tunnel Profile and Cross Sections

The tunnel was extensively instrumented with thermocouples, bi-directional pitot tubes, and video cameras. The sensing equipment was stationed at instrument loops located throughout the tunnel. The loops are described below in Table 1. The fires were generated by burning controlled amounts of No. 2 distillate fuel oil in steel fire pans, located approximately 240 m from the south portal. The fuel oil was pumped to the pans from a remote location. Continuous measurements of the fuel flow rate, fire pan weight, and combustion product gas concentrations were used to compute the fire heat release rate. The combustion efficiency of the fire was estimated from CO and CO_2 concentrations sampled at the ceiling level, approximately 60 m away from the fire.

Table 1 Instrument Loop Descriptions

Loop Number	Distance from North Portal	Sensing Equipment			
		Velocity	Temperature	Gas	TV Camera
214	20 m	X	X	X	
213	106 m		X		
211	211 m		X		
209	321 m	X	X	X	
208	426 m	X	X		
207	508 m	X	X	X	
307	554 m	X	X	X	X
306	586 m		X		
305	604 m	X	X		
205	615 m		X		
304	628 m	X	X		
303	645 m		X		
302	682 m	X	X	X	X
301	723 m	X	X	X	
202	834 m	X	X	X	

3.2 Longitudinal Ventilation Testing Phase

During this testing phase, both cold flow tests and fire tests were performed. The cold flow tests were performed to establish the relationship between the number of fans in operation and the induced airflow in the tunnel. A total of 15 fire tests, with nominal heat release rates of 10, 20, 50 and 100 MW, were conducted to cover a range of fire sizes. These tests evaluated the ability of jet fan ventilation system to control the spread of smoke and heat under the influence of a number of parameters including fire heat release rate, fan response time, and the number of fans in operation. Outside conditions including wind speed and direction and air temperature were recorded during each test so that their impact on ventilation system performance could be evaluated.

4 MODEL VALIDATION

In the first stage of model validation, the jet fan model was used to compute isothermal flows in prototype tunnels. These simulations, which are fully discussed in Ref. 4, show that model predictions are in accordance with established jet fan/tunnel flow performance relationships, and in reasonable agreement with other published information. After the initial verification, the model was used to simulate the tests from the Memorial Tunnel program.

The first step in the application of the model to the Memorial Tunnel tests was to ensure that the model correctly reproduced the tunnel's overall resistance to airflow. The effective tunnel resistance was independently determined from an airflow die-down test. A CFD representation of the tunnel geometry and obstructions was then developed and tested to reflect this overall resistance. The jet fan model was then tested by simulating various cold flow tests. The validation process continued with the simulation of full-scale fire tests. Four tests with nominal fire heat release rates of 10, 20, 50 and 100 MW were selected for validation. Steady-state simulations of the tests were performed, and their results were compared with test data averaged over portions of the observed quasi steady-state periods. Transient simulations were performed to test the model's ability to predict unsteady conditions that result from changes in fan operation and fire heat release rate.

4.1 Determination of the Effective Tunnel Resistance

Since the flow generated by a jet fan system is fixed by the balance point of the pressure rise produced by the fans and the pressure drop due to tunnel resistance, it was essential to establish this value in the validation process. The tunnel's effective resistance to airflow reflects the combined effects of: (1) the obstructions in the tunnel; (2) changes in tunnel geometry; (3) tunnel wall surface roughness; and (4) tunnel inlet and exit losses. The data collected during a die-down test (resistance test B) was used to determine the effective tunnel resistance. During this cold flow test, 15 jet fans were operated in unison and, once conditions in the tunnel stabilized, all the fans were deactivated. Air velocities throughout the tunnel were recorded as the flow attenuated and returned to ambient conditions. An analysis of this data indicated a loss coefficient equal to 13.1, based on the large tunnel cross-sectional area, was appropriate to represent the tunnel's effective resistance to airflow.

4.2 Tunnel Representation

Once the resistance of the tunnel was established, the CFD representation of the tunnel geometry was developed. The installation of data collection and communication equipment, video cameras, fire pans, and support systems throughout the tunnel introduced considerable obstruction in the tunnel roadway, particularly in the regions where most of the data was collected. It was important, therefore, to include these elements as solid objects in the model since they not only introduced resistance into the tunnel model but also affected the velocity data. To this end, a number of simple flows around obstructions were computed to ensure that flow losses due to these obstructions were correctly predicted. Once an appropriate means for modeling each component, including grid representation, was determined, all components were combined and a number of cold flow simulations were made to confirm that the total effective resistance of the model agreed with the value obtained from the die-down test.

For the results presented here, the tunnel was represented by a structured Cartesian non-uniform grid consisting of 29 cells in the width direction, 25 cells in the height direction, and 338 cells in the longitudinal direction. The tunnel portals were modeled as given-pressure boundaries. The tunnel walls were assumed to be isothermal, except for a 120 m long section in the vicinity of the fire. The walls in this area were sprayed with several centimeters of insulation as a protective measure. This region was taken as adiabatic. The tunnel walls were assigned a roughness height similar to that of rough concrete.

4.3 Validation Simulations: Cold Flow Tests

During phase III of the MTFVTP, a number of cold flow tests were performed in which different combinations of jet fans were operated and bulk flow measurements at each loop were recorded once the flow stabilized. In tests with the same number of operating fans, different combinations of fans were used to identify any differences associated with location of jet fans or between fans operating in parallel or series arrangements. Some fans were located close to instrument loops and it was conceivable that their performance could be adversely affected by local obstructions. The results of the cold flow tests with 3, 9, and 15 fans in operation are presented in Table 2. The bulk flow rates listed were measured at the north portal of the tunnel (loop 214). The placement of jet fans in the tunnel is shown in Figure 2.

Table 2 Cold Flow Test Results

Test Number	No. of Fans Operating	Fans Utilized	Bulk Flow (m^3/s)	Average Bulk Flow (m^3/s)
3	3	G6	185	
7	3	G8	179	
1	3	F5, F14, F23	177	175
A2	3	F2, F8, F14	169	
D3	3	G3	165	
11	9	G1–G3	284	288
C2	9	G1, G3, G5	293	
C4	15	G1–G5	372	376
Resistance	15	G1–G5	380	

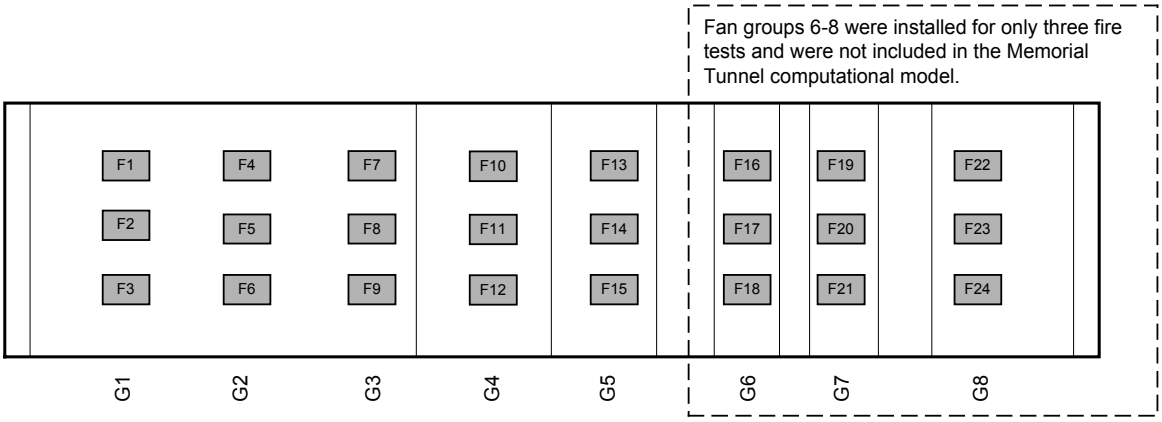

Figure 2 Jet Fan Placement in the Memorial Tunnel

For a given number of operating jet fans, the measured nominal bulk flow rates vary from test to test. These variations may be due, in part, to natural flow through the tunnel caused by differences in meteorological conditions at the portals and/or buoyancy forces due to the temperature difference between the tunnel walls and the ambient air. However, pre-test conditions were not recorded during cold flow tests and it is difficult to identify precise causes of this variability.

The predicted bulk flow rates in the cold-flow simulations with 3, 9, and 15 jet fans in operation are compared with the test data in Table 3. An analysis of the test data failed to indicate any significant differences that could be attributed specifically to fan location or operation. Therefore, calculated bulk airflow rates are compared with the average measured values.

Table 3 Comparison of CFD Simulation Results with Data for Cold Flow

No. of Fans Operating	Test Data	CFD Model		Deviation from Test Data (%)
	Average Bulk Flow (m^3/s)	Fans Utilized	Bulk Flow (m^3/s)	
3	175	G1	183	4.6
9	288	G1–G3	310	7.4
15	376	G1–G5	394	4.6

There is a good agreement between the calculated results and the test data, with a maximum discrepancy of less than 8 percent. The possible variations in the ambient conditions, discussed earlier, were not accounted for in these simulations. Due to lack of data on pre-test conditions, it was difficult to include this element in the model without introducing additional uncertainty.

4.4 Validation Simulations: Fire Tests

Four tests representing nominal heat release rates of 10, 20, 50, and 100 MW were chosen to evaluate the model for fire scenarios. For sake of brevity, only selected results for the 10 and 100 MW tests are presented; complete results for all four tests are available in Ref. 4.

4.4.1 Test 606A

Test 606A, a nominal 10 MW test, was conducted with 15 jet fans installed in the tunnel. Full pan engulfment occurred 56 s after fuel ignition. Initially there was no mechanical ventilation. Jet fans F3 and F6 (see Figure 2) were activated 304 s and 319 s after the full pan engulfment. This fan setting was maintained for 20 minutes, at which time another jet fan was turned on. During the initial period of natural ventilation, which lasted 6 minutes, smoke and heat propagated upgrade and moved out from the north portal. The flow was reversed shortly after two jet fans were activated and tunnel conditions stabilized approximately 11 minutes after the fan activation.

Steady-State Simulations. A steady-state simulation was made to reproduce the stable conditions observed after the jet fans were activated. A convective heat release rate of 6.4 MW was used, which was estimated from the data for fuel consumption rate and combustion efficiency with a value of 0.3 for the radiative fraction. The wall surface temperature was taken to be 10°C above the ambient temperature. A differential pressure was specified between the tunnel portals to supplement the buoyancy effect generated by the exchange of heat at the tunnel walls to produce the initial south-to-north airflow observed in the test prior to the start of the fire.

Figure 3 presents the comparison of the predicted and measured bulk flow rates and temperatures. The agreement between the two sets of results is good, except in the immediate vicinity of the fire. The large discrepancies near the fire are partly due to radiation error in temperature measurement using unshielded thermocouples and partly due to the simplified representation of fire as a heat source, which is less satisfactory near the fire. At loop 303, located 30 m downstream of the fire, the predicted bulk temperature is 11°C lower than the measured value; this difference reduces to less than 2°C near the south portal. Figure 4 shows the comparison of the velocity and temperature profiles at selected locations on the mid plane of the tunnel. The close agreement between the predictions and the measurements demonstrates the ability of the model to correctly reproduce global quantities as well as the local details of this test.

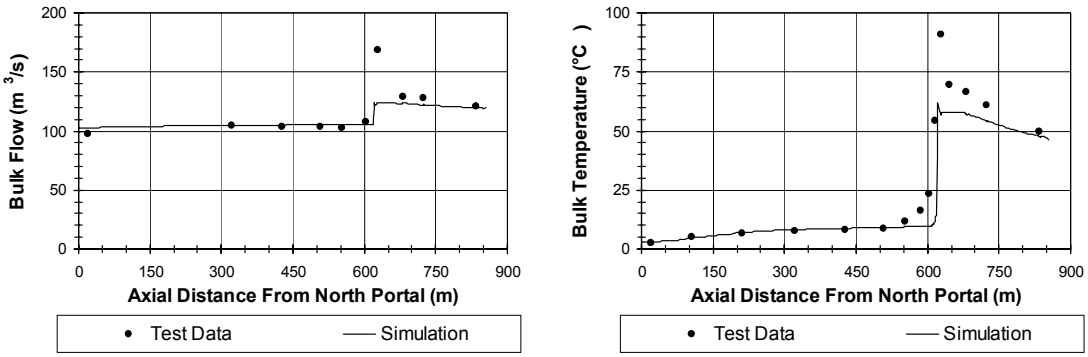

Figure 3 Bulk Flow and Temperature Distributions for Test 606A (Steady State)

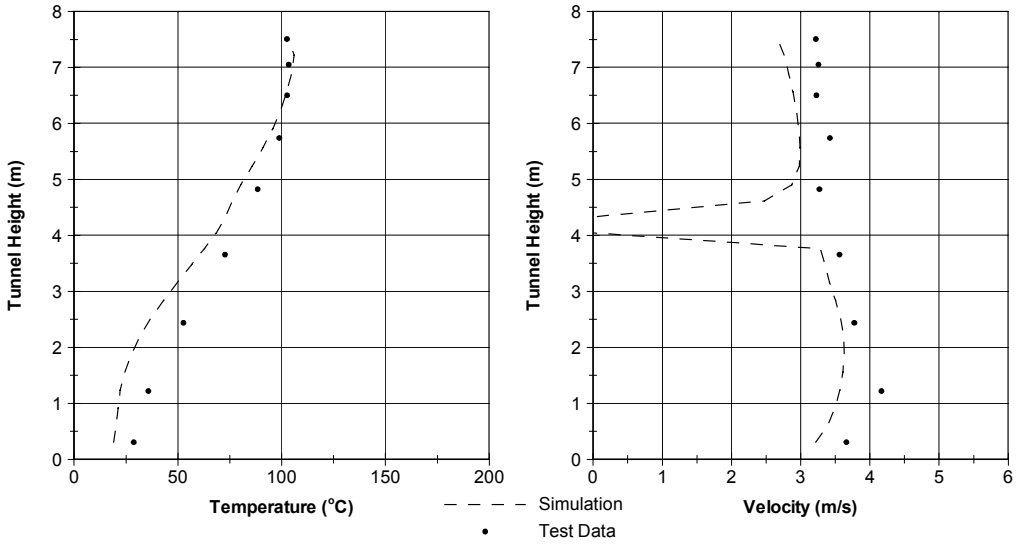

(a) Loop 302 (66 m south of fire site)

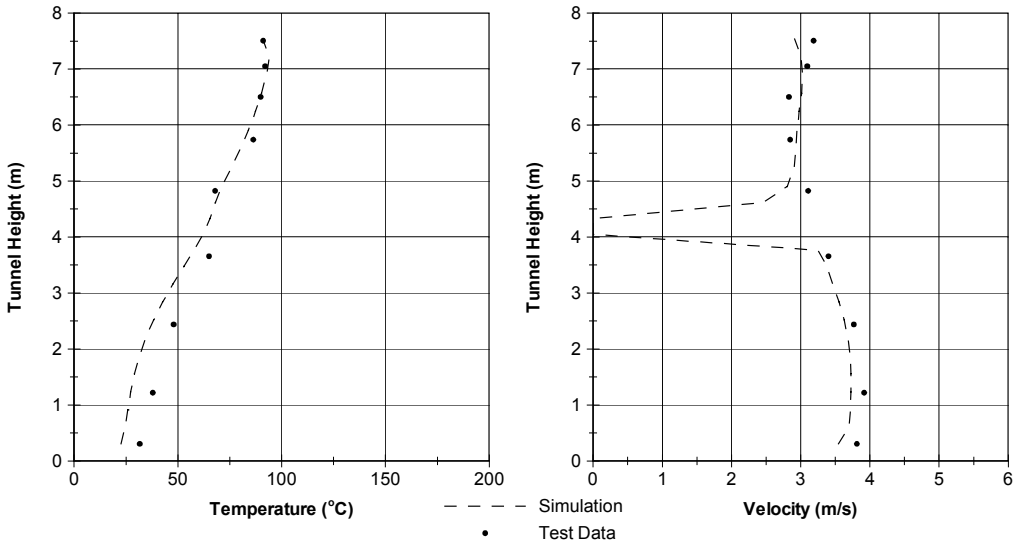

(b) Loop 301 (108 m south of fire site)

Figure 4 Temperature and Velocity Profiles for Test 606A (Steady State)

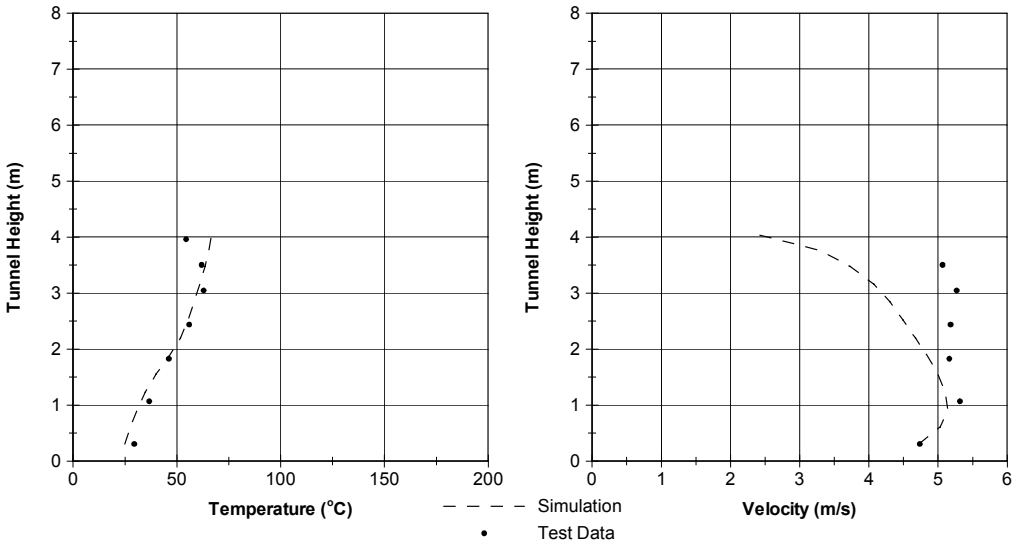

(c) Loop 202 (219 m south of fire site)

Figure 4 (*Continued*) Temperature and Velocity Profiles for Test 606A (Steady State)

Transient Simulations. The objective of the transient simulations was to verify if the model could mimic the test results for the delayed fan response and the subsequent steady-state conditions. In these simulations, the ambient flow through the tunnel prior to the test served as the initial condition.

The first attempt for a transient simulation was based on the heat release rate profile designated as T1 in Figure 5. These results, discussed in Ref. 4, did not agree with the test data and indicated that the fan system was unable to overcome the buoyancy forces generated by the fire. To understand the reasons for the failure of the model, additional parametric runs were made. These results indicated that the predicted flow field in the tunnel was sensitive to the heat release rate profile. This behavior is not surprising because the air velocity is close to the critical velocity, as evidenced by the small backlayer during the quasi steady-state period, and the tunnel conditions represent a balance between buoyancy forces and flow inertia. Slight changes in the operating conditions, especially the heat release rate, can disrupt this balance and can lead to very different flow fields. Thus, it is important to specify a reasonable heat release rate profile. In this simulation, however, this task became difficult due to the erratic behavior of the heat release rate at the beginning of the test. The parametric runs indicated that the simulation using the heat release rate profile designated as T2 in Figure 5 was successful in reproducing much of the test data.

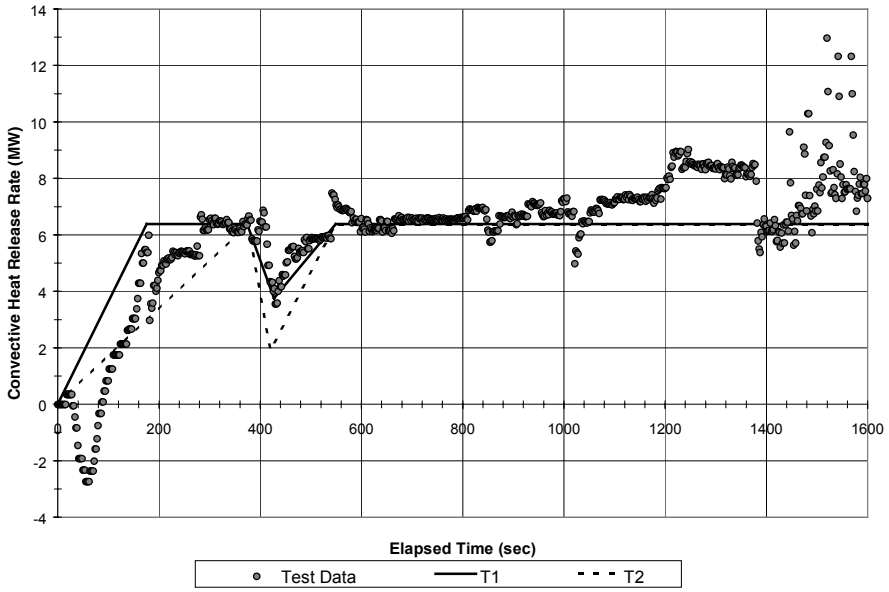

Figure 5 Measured and Simulated Heat Release Rate Profile for Test 606A

These results are presented in Figures 6 and 7. Figure 6 is a series of plots in which the predicted bulk flow rates vs. time at selected loops are compared with the measured values. Figure 7 includes selected comparisons of measured and predicted distributions of temperature and smoke. The smoke distribution for the test was estimated from the smoke front locations observed on the video captured by the CCTV system installed in the tunnel; for the simulation, it is based on the visibility contours deduced from the smoke concentrations. The visible edge of the smoke front corresponds to regions where the smoke dilution levels lie between 100:1 and 500:1 of the maximum smoke concentration at the fire site. In test 606A, these dilution levels correspond to a visible range between 45 m and 140 m.

Prior to the activation of the jet fans, the combined effects of fire, tunnel wall-to-ambient temperature difference, and differential portal pressures generate a south-to-north flow through the tunnel. The predicted bulk flow rates at the start of the test and just prior to the activation of the first jet fan agree well with the test data. In between, however, the predicted bulk flow rates are lower than the test data, with a maximum difference of 25%. This disparity may be due to a nonlinear fire growth in the test. (Also note that during this period the measured heat release rate shows an erratic behavior and the specified heat release rate curve is approximate.) Overall, the predictions for natural ventilation compare reasonably well with the test results.

Following fan activation, the hot gases and smoke north of the fire are forced southward. During the initial recovery period, Figure 7(b), the elevated temperatures north of the fire, in both the simulation and the test, remained stratified to the same degree that they were prior to the fan activation, Figure 7(a). Smoke was not stratified during the natural ventilation period; after fan activation, smoke was forced southward, filling the entire tunnel cross section. As both the test and simulation progress further, the conditions in the tunnel become steady. The predicted smoke front location agrees well with the test observations.

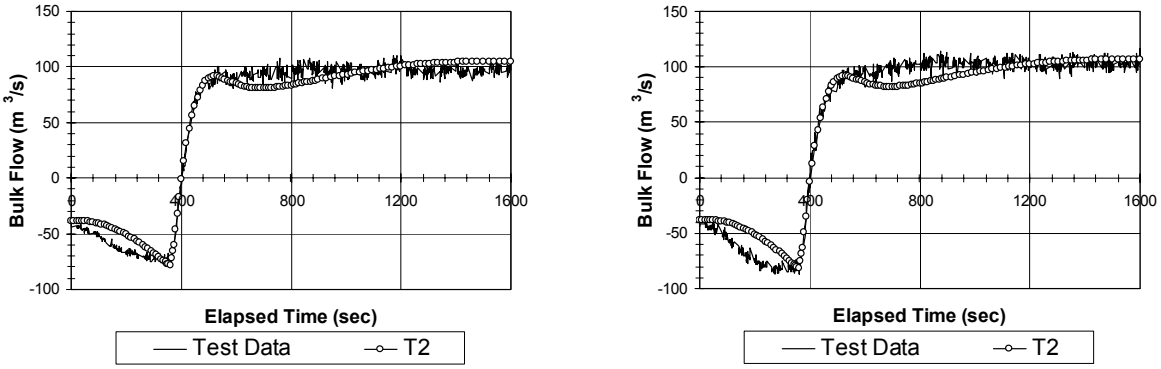

(a) Loop 214 (596 m north of fire site)

(b) Loop 207 (107 m north of fire site)

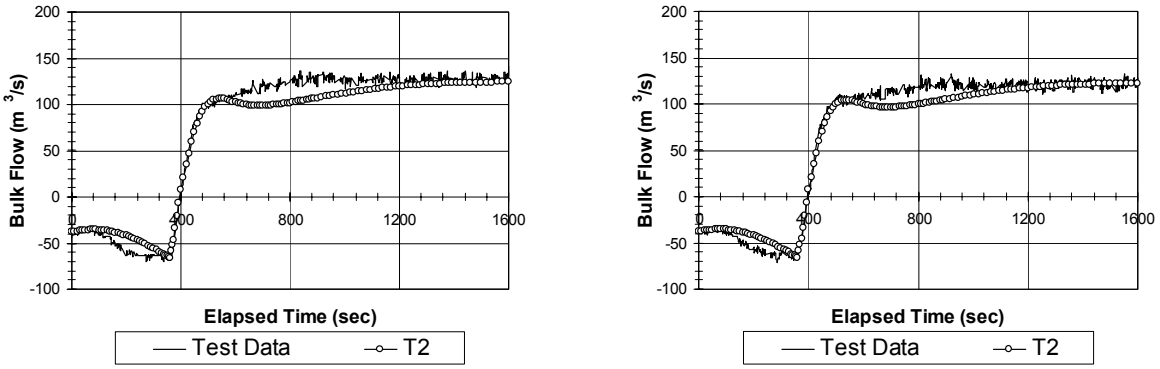

(c) Loop 301 (108 m south of fire site)

(d) Loop 202 (219 m south of fire site)

Figure 6 Measured and Predicted Bulk Flow Rates for Test 606A (Transient)

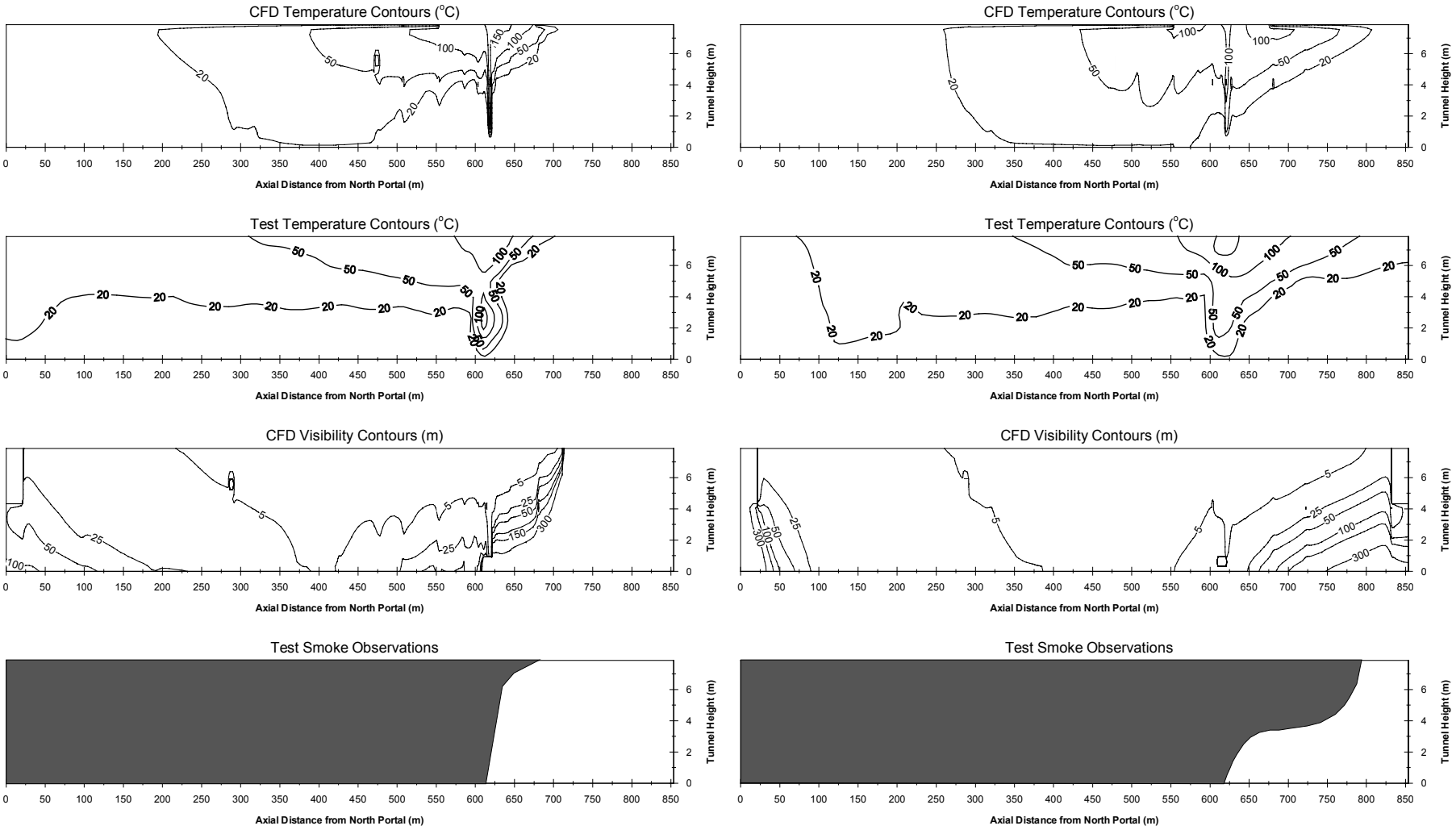

(a) Time 360 s

(b) Time 450 s

Figure 7 Temperature and Visibility Contours for Test 606A (Transient) at: (a) 360 s; (b) 450 s

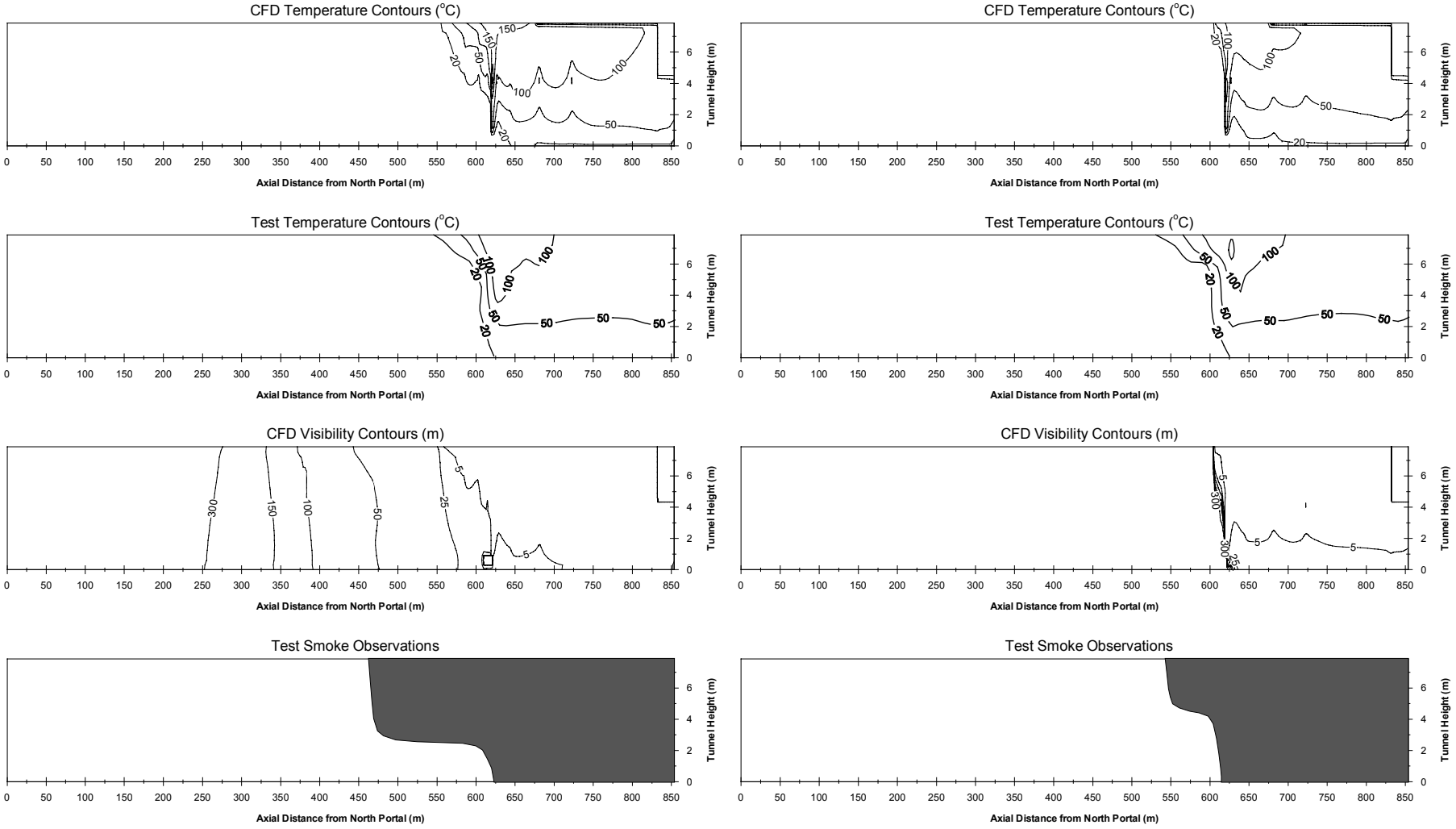

(c) Time 870 s (d) Time 1,245 s

Figure 7 (*Continued*) Temperature and Visibility Contours for Test 606A (Transient) at: (c) 870 s; (d) 1,245 s

4.4.2 Test 615B

Test 615B, a nominal 100 MW fire test, was used to validate the model at the high end of the heat release rates tested. This test was also conducted with 15 jet fans installed. Six jet fans were activated 2 minutes after full pan engulfment. There was no backlayering during the resulting steady-state period. Twelve minutes later, one jet fan was deactivated for 8 minutes, resulting in backlayering for the second quasi steady-state period. The sequence of events in this simulation is listed in Table 4. The measured and simulated heat release rate profiles are shown in Figure 8. This test included steady-state periods with and without backlayering. In addition, the test involved a delay in fan activation and changes in fan operation. These features made this test a good scenario for assessing the capabilities of the model.

Table 4 Sequence of Events for Test 615B

Event	Elapsed Time (s)
Start of Test	0
Fans 1, 3, 4, 6, 7 and 9 activated	188
Fan 7 deactivated	901
Fans 7 activated	1385

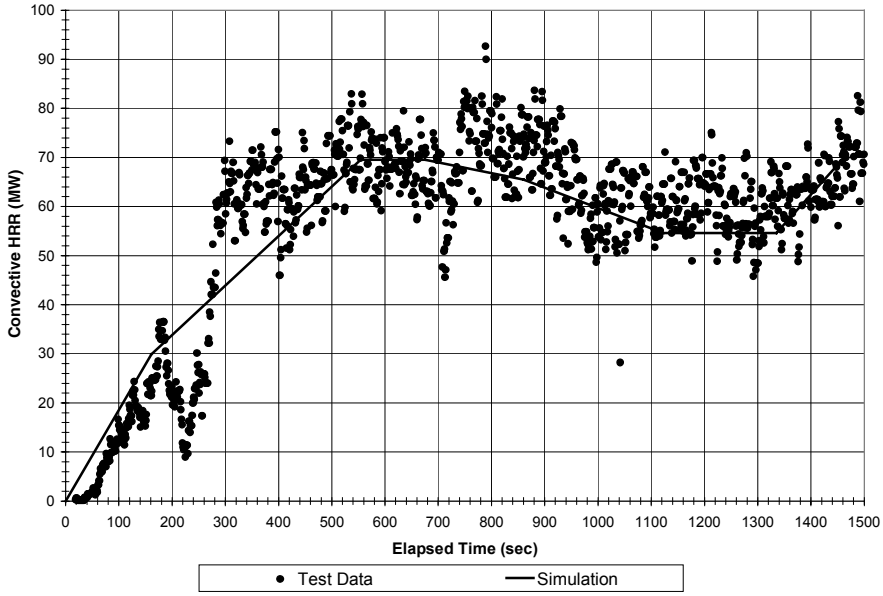

Figure 8 Measured and Simulated Heat Release Rate Profile for Test 615B

Steady-State Simulations. A steady-state simulation (Steady State I) was performed to reproduce the controlled conditions observed after 6 jet fans were activated. This simulation used a convective fire heat release rate of 69.5 MW, estimated using a value of 0.3 for the radiative fraction. The wall surface temperature was taken to be 7.7°C above the ambient temperature. Differential pressures were prescribed on the portals to produce an ambient south-to-north airflow prior to the start of fire, as observed in the test.

Figure 9 presents the comparison of the predicted bulk flow rates and temperatures with the test data. North of the fire, the calculated results are in good agreement with the measured values. South of the fire, however, the model underpredicts the test data for the first 60 m; beyond this point, the agreement is again good.

The discrepancies just south of the fire may be attributed to a combination of the radiation error in the temperature measurements and the simplified representation of fire, which does not include models for combustion and radiation. For larger fires, where smoke and soot concentrations are high, the local absorption and emission of radiation becomes important. Based on an average temperature of about 550°C and analysis of CO_2 concentration levels and soot volume fractions generated by the fire for this test, it is estimated that a significant portion of the radiation emitted by the flame would be absorbed locally by the products of combustion (gases and soot), instead of being directly transferred to the walls as assumed in the model. Eventually, this energy is transferred to the walls beyond the fire region, as indicated by the test results.

The predicted and measured velocity and temperature profiles are in good agreement north of the fire and are not shown here. Figure 10 presents the comparison of the profiles at selected locations south of the fire. In this region, the model predicts a higher degree of thermal stratification. This pattern is consistent with the behavior of the bulk quantities discussed above.

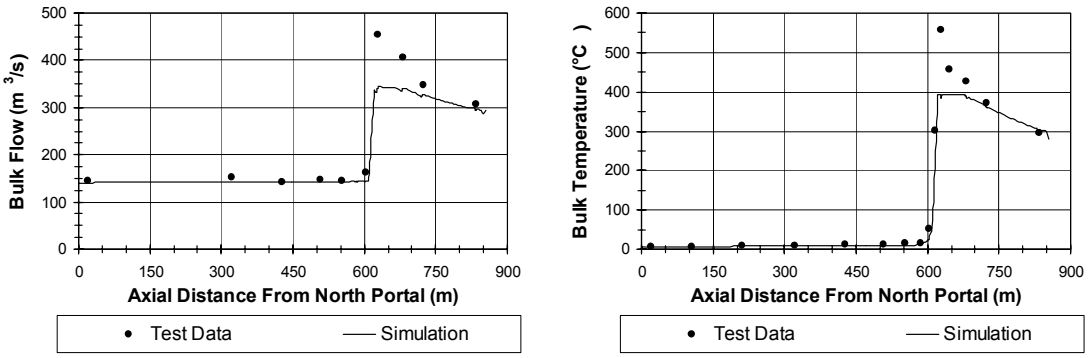

Figure 9 Bulk Flow and Temperature Distributions for Test 615B (Steady State I)

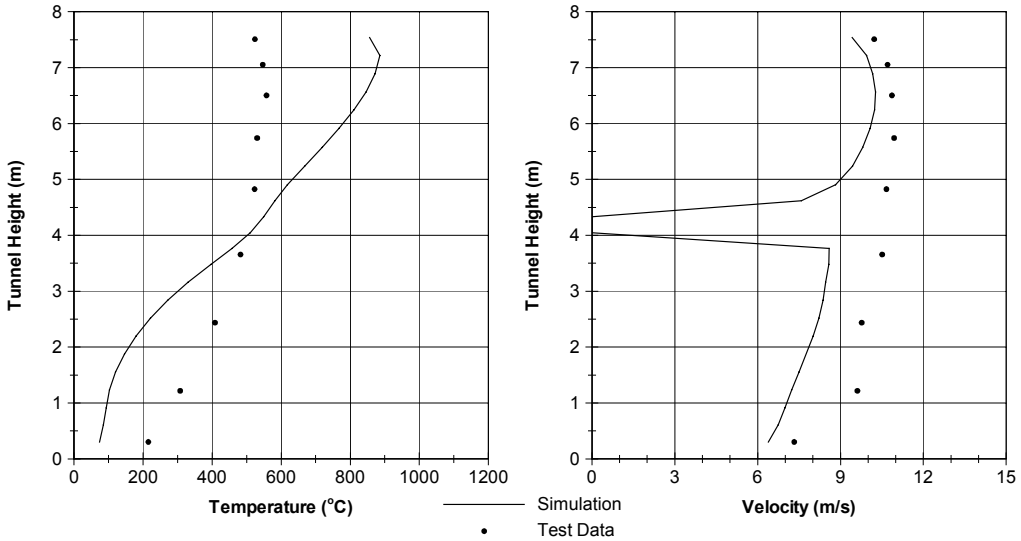

(a) Loop 302 (66 m south of fire site)

Figure 10 Temperature and Velocity Profiles for Test 615B (Steady State I)

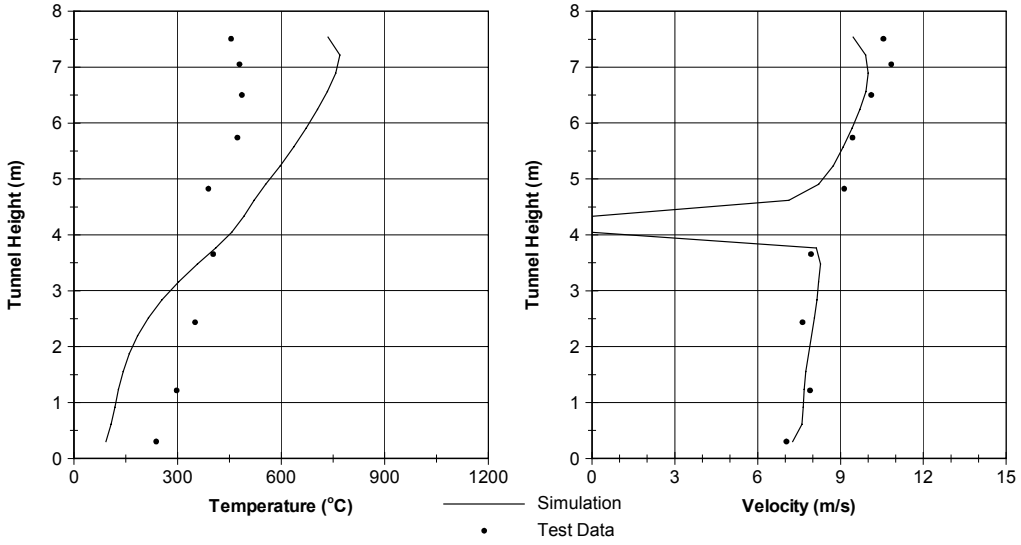

(b) Loop 301 (108 m south of fire site)

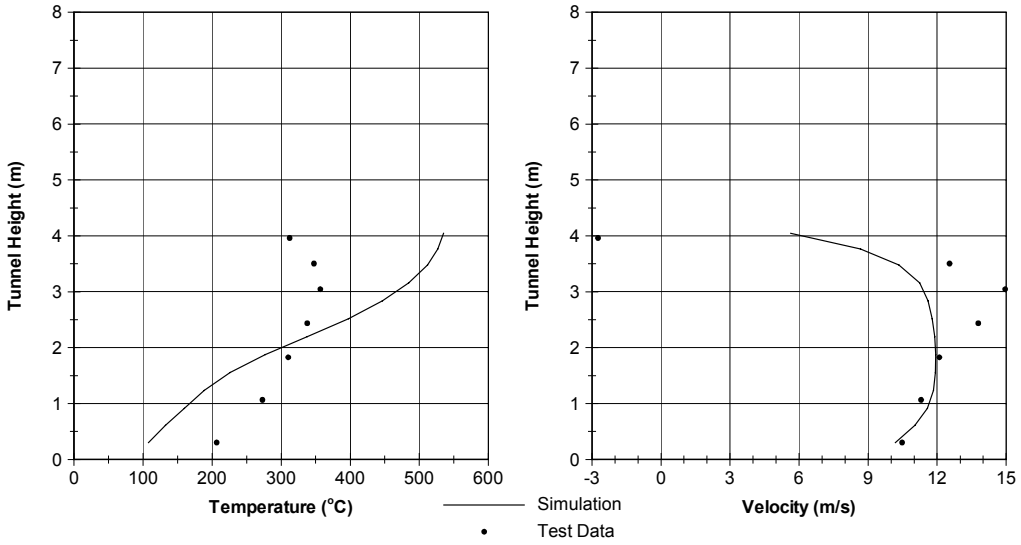

(c) Loop 202 (219 m south of fire site)

Figure 10 (*Continued*) Temperature and Velocity Profiles for Test 615B (Steady State I)

Another steady-state simulation (Steady State II) was made to check if the model could predict the steady backlayer observed when the number of operating jet fans was reduced from 6 to 5. Convergence was difficult to achieve in this simulation. Only when the differential portal pressure was removed and the simulated convective heat release rate was reduced to 54.5 MW (10% less than the value estimated from the data) was a converged solution obtained.

Figure 11 shows the comparison of predicted and measured bulk quantities. The temperature of the approaching air compares well with the test data, except in the backlayer region north of the fire. The model underpredicts the bulk flow rate of the incoming air by approximately 10%. As in the earlier simulation, there are significant differences south of the fire. However, as the hot gases exit the tunnel, the ratio of predicted to measured flow rates at the south portal is about the same as that on the north side of the fire. The predicted bulk temperature at the south portal is about 45°C higher than the measured value. The combination of lower flow rate and higher

temperature at the exit portal suggests that the heat release rate specified in the simulation may have been slightly overestimated.

Figure 12 presents the comparison of the predicted temperature and smoke distributions with the test data. In this simulation, the smoke front location corresponds to visibility contours between 18 m and 54 m. The temperature and visibility levels in the backlayer are well predicted, but the calculated length and depth of the backlayer are larger than the measured values.

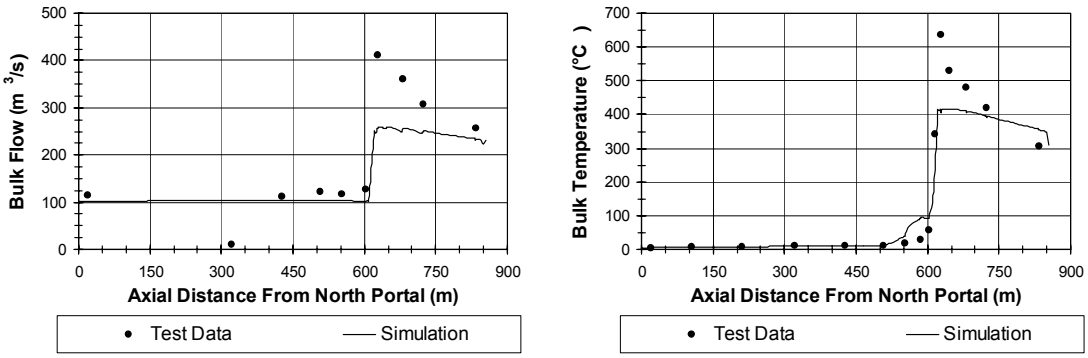

Figure 11 Bulk Flow and Temperature Distributions for Test 615B (Steady State II)

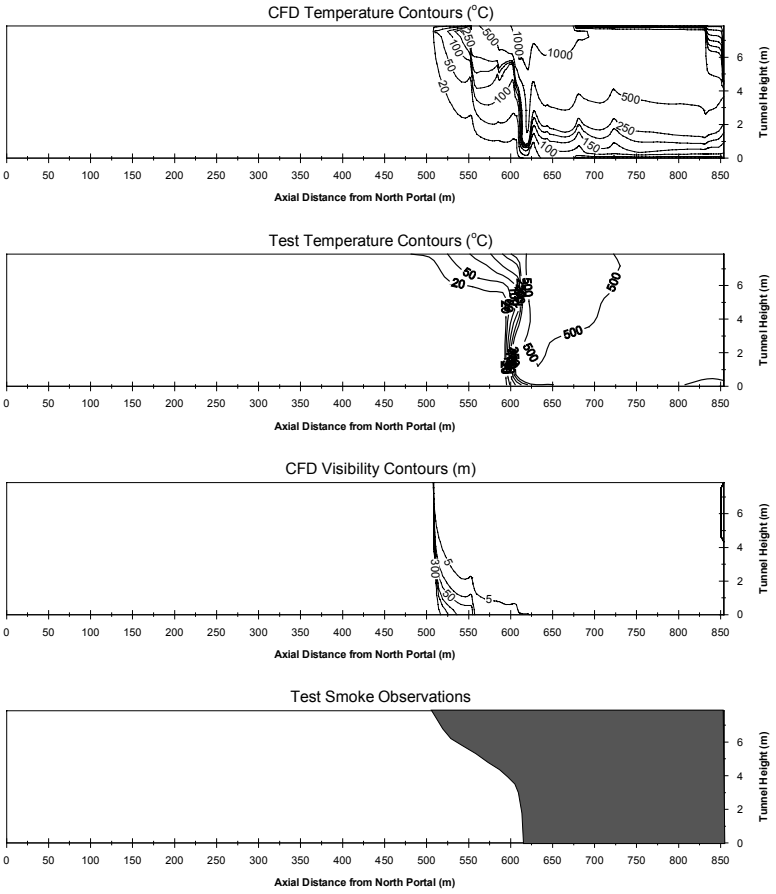

Figure 12 Temperature and Visibility Contours for Test 615B (Steady State II)

Transient Simulations. The transient simulation of test 615B covers the 25-minute period between fuel oil ignition and fuel shut off. The objective of the simulation was to verify if the model could reproduce the tests results for the delayed fan response and the subsequent transitions between 6 and 5 jet fans operating. Consistent with the steady-state simulation with 5 operating jet fans, the differential pressure between the portals was removed when the number of fans was changed from 6 to 5.

Figure 13 shows the comparison of the predicted and measured bulk flow rates at selected loops. Prior to jet fan activation, the predicted bulk airflow is within the bandwidth of test data. Once the jet fans are activated, the predicted and measured bulk flow rates rapidly increase during the first 400 seconds and then attenuate to the condition achieved during the first steady-state period. During this period, with 6 fans in operation, the agreement between the predictions and test data is good. After one fan is turned off at 860 seconds, the flow through the tunnel reduces and then achieves another steady state. For the second steady-state condition, the bulk flow rate is slightly underpredicted.

Figure 14 shows the comparison of the temperature and visibility contours at selected points in time. In the simulation, the smoke front location corresponds to a visibility range between 18 and 55 m. During the initial recovery period, Figures 14(a) and 14(b), the model predicts a greater degree of mixing (less stratification) north of the fire. The extent of the hazardous region is predicted well. For the quasi steady-state conditions, Figure 14(c), the agreement between the predictions and measurements is good. When one jet fan is deactivated, backlayering occurs as seen in Fig. 14(d). The extent of the backlayer is well predicted, but the calculated depth of the layer is larger than in the test. Although not shown here, the events following the reactivation of a jet fan are also predicted with good accuracy.

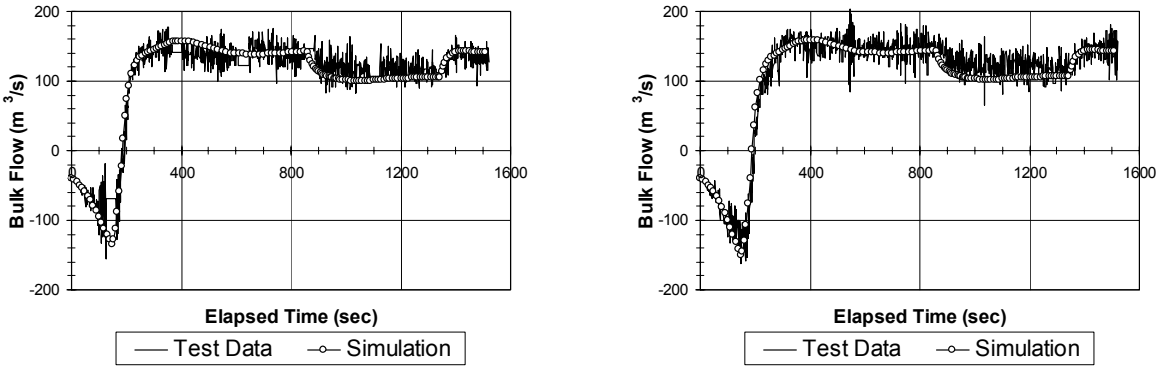

(a) Loop 214 (596 m north of fire site)

(b) Loop 207 (107 m north of fire site)

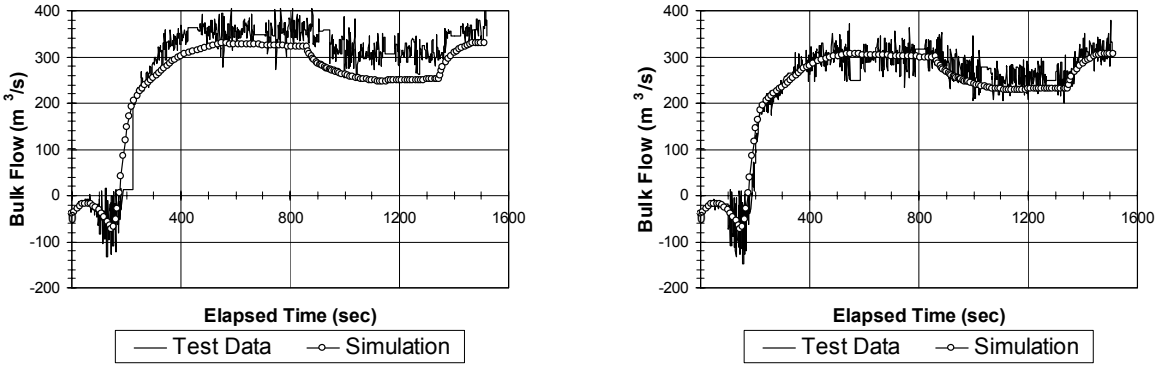

(c) Loop 301 (108 m south of fire site)

(d) Loop 202 (219 m south of fire site)

Figure 13 Measured and Predicted Bulk Flow Rates for Test 615B (Transient)

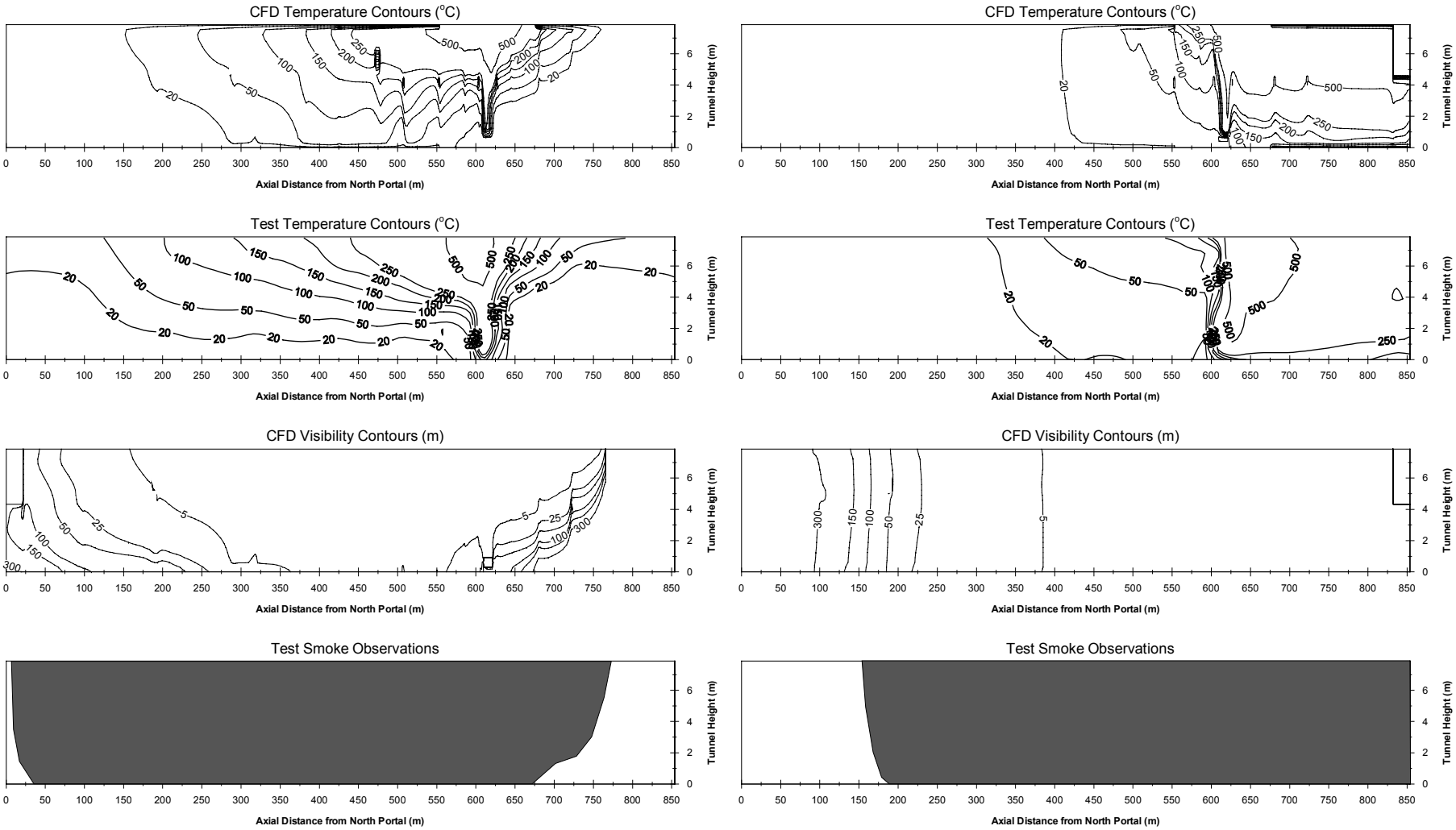

(a) Time 147 s

(b) Time 330 s

Figure 14 Temperature and Visibility Contours for Test 615B (Transient) at: (a) 147 s; (b) 330 s

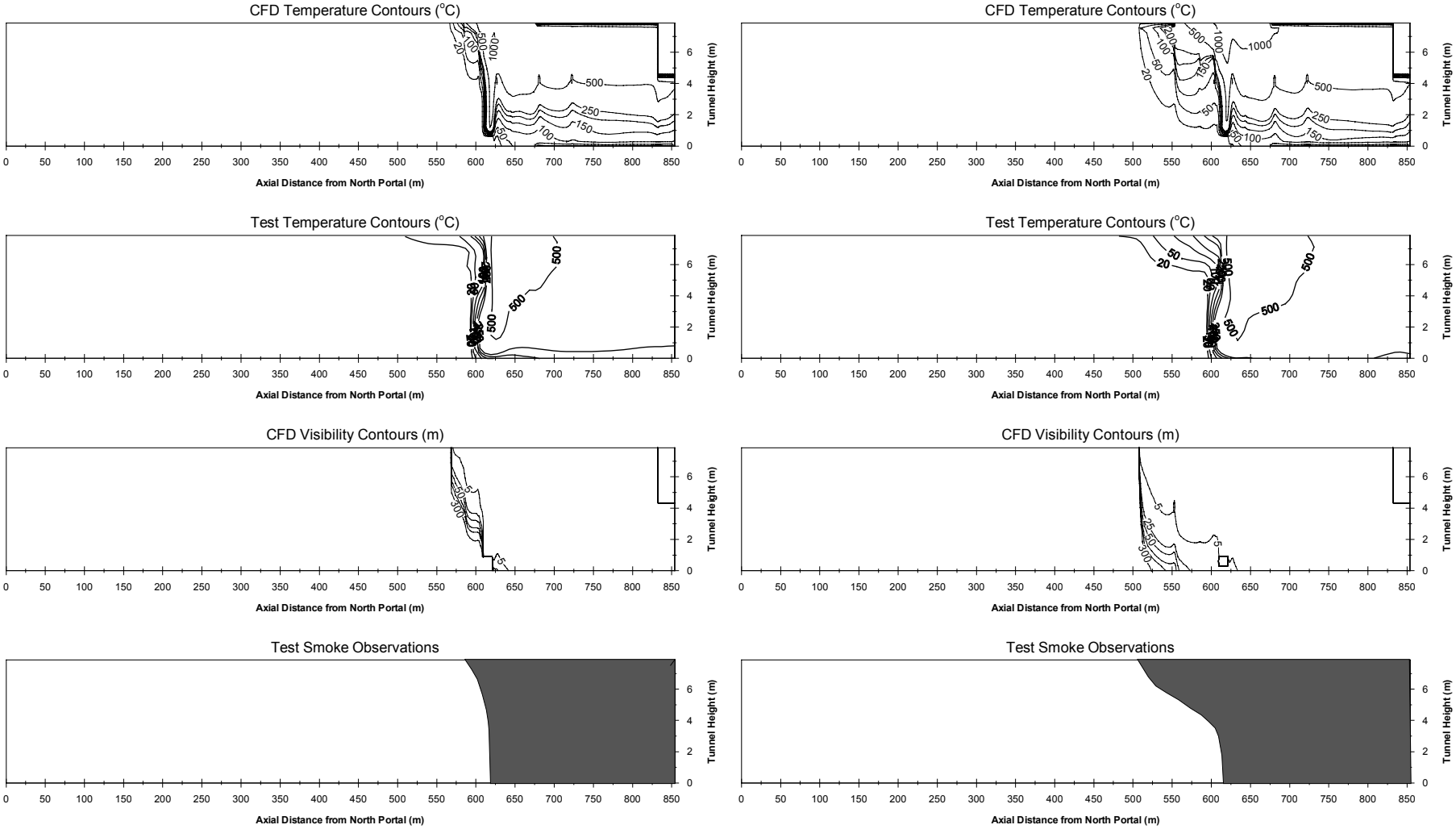

(c) Time 700 s (d) Time 1,300 s

Figure 14 (*Continued*) Temperature and Visibility Contours for Test 615B (Transient) at: (c) 700 s; (d) 1,300 s

5 CONCLUDING REMARKS

This paper gives the details of the development and validation of a mathematical model, based on computational fluid dynamics, for a longitudinal ventilation system using jet fans. The model has been extensively validated using the test data from the Memorial Tunnel Fire Ventilation Program. The key findings of the work reported here are:

- The model correctly predicts the airflow generated by a jet fan ventilation system.
- The simplified approach of representing the fire as a volumetric heat source and neglecting the radiation component of the fire heat release rate is adequate for predicting the effects of the fire in the far-field region of the tunnel, i.e., more than 60 m away from the fire. Within the uncertainty in the fire heat release rate, the predicted values of bulk flow, bulk temperature, and, in most cases, temperature/velocity profiles are in good agreement with test data. As would be expected, comparisons are not as favorable near the fire. The results for the steady-state simulations indicate:
    1. Upstream of the fire, where the air is essentially at ambient temperature, the bulk flow predictions are within 10 percent of the measured values.
    2. Downstream of the fire, bulk flow predictions are mostly within 15 percent of the measured data; predicted bulk temperatures are within 10 percent.
    3. With the exception of the 100 MW fire test, temperature and velocity profiles compare well with the test data. For large fires, the level of temperature stratification is significantly overpredicted.
- The model correctly predicts the extent and location of the hazardous region as a function of fire size, fan capacity, and fan operation, under both steady state and transient conditions. In particular:
    1. The occurrence of a steady backlayer condition is predicted correctly. The extent of the backlayer (distance from the fire) is sensitive to the heat release rate. The depth of the backlayer below the ceiling is generally overpredicted.
    2. The transition between controlled and uncontrolled conditions, caused by a reduction in fan capacity, is correctly predicted. When the jet fan system capacity was reduced in a test, resulting in a backlayer condition, the model reproduced the observed phenomena in a transient simulation.
    3. The predictions of the rate and extent of smoke and high temperature propagation in the upgrade direction due to buoyancy, and its subsequent reversal due to jet fan system activation, show good agreement with test observations.
    4. Predicted regions of optically dense smoke agree with video camera recordings of the smoke front locations.

These findings indicate that the model adequately addresses the physics associated with the interaction of a fire and a jet fan ventilation system, under both steady and transient conditions.

ACKNOWLEDGEMENTS

The authors thank Mr. Jason Sandzimier, Parsons Brinckerhoff, for his thorough review of the manuscript and assistance in its preparation.

REFERENCES

1. Massachusetts Highway Department and Bechtel/Parsons Brinckerhoff, Memorial Tunnel Fire Test Ventilation Program – Test Report, 1995.
2. Innovative Research, *Reference Manual for COMPACT-3D*, Innovative Research, Inc., Minneapolis, 1998.
3. Levy S., Sandzimier, J., Harvey, N., Rosenbluth, E., Karki, K., and Patankar, S., CFD Model for Transverse Ventilation Systems, *Tunnel Fires and Escape from Tunnels*, International Conference, Lyons, France, 1999, pp. 223–233.
4. Massachusetts Highway Department/Federal Highway Administration, *Memorial Tunnel Fire Ventilation Test Program, Phase IV Report*, 1999.
5. Armstrong, J., Bennet, E. C., Matthews, R. D., Smith, T. W., and Tabarra, M., The Ventilation of Vehicle Tunnels by Jet Fans—The Axisymmetric Case, *Proceedings of the Seminar on Installation Effects in Fan Systems*, Mechanical Engineering Press, London 1993, pp. 59–64.
6. Tabarra, M., Bennet, E. C., Matthews, R. D., Armstrong, J., and Smith, T. W., Eccentricity Effects on Jet Fan Performance in Longitudinally Ventilated Rectangular Tunnels, Paper presented at the *I. Mech. E. Seminar Fans for Hazardous Applications*, London, 1994.
7. Tabarra, M., Bennet, E. C., and Matthews, R. D., Optimizing Jet Fan Performance in Longitudinally Ventilated Rectangular Tunnels, *Separated and Complex Flows*, ASME FED-Vol. 217, 1995, pp. 35–42.
8. Miles, S. and Kumar, S., Validation of a CFD Model for Fires in the Memorial Tunnel, *Tunnel Fires and Escape from Tunnels*, International Conference, Lyons, France, 1999, pp. 150–168.
9. Patankar, S. V., *Numerical Heat Transfer and Fluid Flow*, Taylor and Francis, 1980.
10. Cox, G., 1995, *Combustion Fundamentals of Fire*, Academic Press, 1995.
11. Launder, B. E. and Spalding D. B., The Numerical Computation of Turbulent Flows, *Computer Methods in Applied Mechanics and Engineering*, Vol. 3, 1974, pp. 269–289.
12. Jayatilleke, C. L. V., The Influence of Prandtl Number and Surface Roughness on the Resistance of Laminar Sub-layer to Momentum and Heat Transfer, *Progress in Heat and Mass Transfer*, Vol. 1, Pergamon Press, 1969, pp. 193–329.
13. Markstein, G. H., Relationship Between Smoke Point and Radiant Emission from Buoyant Turbulent and Laminar Diffusion Flames, *20th Symposium (International) on Combustion*, The Combustion Institute, Pittsburgh, 1984, pp. 1055–1061.
14. Patankar, S. V. and Spalding, D. B., A Computer Model for Three-Dimensional Flow in Furnaces, *14th Symposium (International) on Combustion*, The Combustion Institute, Pittsburgh, 1972, pp. 605–614.
15. Patankar, S. V., Karki, K. C., and Kelkar, K. M., Finite Volume Method, in Johnson, R.W., Ed., *The Handbook of Fluid Dynamics*, CRC Press, 1998.
16. Settari, A. and Aziz, K., A Generalization of the Additive Correction Methods for the Iterative Solutions of Matrix Equations, *SIAM Journal of Numerical Analysis*, Vol. 10, 1973, pp. 506–521.